Available online at www.sciencedirect.com
SCIENCE DIRECT®
Biochimica et Biophysica Acta 1611 (2003) 171–179
BIOCHIMICA ET BIOPHYSICA ACTA
BBA
www.bba-direct.com

Characterization of Zn^{2+} transport in Madin-Darby canine kidney cells

Olivier Ducoudret, Olivier Barbier, Michel Tauc*, Marianne Fuchs, Philippe Poujeol

UMR-CNRS 6548, Université de Nice-Sophia Antipolis, Parc Valrose, 06108 Nice Cedex, France

Received 13 November 2002; received in revised form 17 January 2003; accepted 28 January 2003

Abstract

The aim of this study was to characterize the mechanism implicated in Zn^{2+} transport in MDCK cells. Trace elements such as Zn^{2+}, Cd^{2+} or Cu^{2+} induced MDCK cell depolarization at the micromolar level as demonstrated by bis-oxonol fluorescence and whole-cell patch experiments. This depolarization was inhibited by La^{3+} and Gd^{3+} and was not related to the activation of Na^+ or Cl^- channels. Uptake of ^{65}Zn was assessed under initial rate conditions. The kinetic parameters obtained at 37 °C were a K_m of 18.9 μM and a V_{max} of 0.48 nmol min^{-1} (mg $protein^{-1}$). Intracellular pH measurements using BCECF probe demonstrated that Zn^{2+} transport induced a cytoplasmic acidification. The cytoplasmic acidification resulting from Zn^{2+} uptake activated Na^+/H^+ antiporter, which allowed for the recycling of protons. These data suggest that Zn^{2+} enters MDCK cells through a proton-coupled metal-ion transporter, the characteristics of which are slightly different from those described for the metal transporter DCT1. This mechanism could be in part responsible of the metal transport evidenced in the distal parts of the renal tubule.

Keywords: Metal transport; Zn^{2+}; MDCK; Cytosolic pH

1. Introduction

Zn^{2+} is an essential metal ion implicated in numerous physiological functions but very little is known about the mechanisms which permits the uptake of this ion along the mammalian nephron. Different mechanisms implicated in the transport of heavy metals have been identified in several types of cells such as intestinal cells, hepatocytes, erythrocytes, endothelial cells, leukocytes and placental trophoblast cells [1]. However, in the kidney, which is one of the main organs implicated in trace element homeostasis in the body, it appears that only proximal cells have been studied [2]. Notably, using isolated renal proximal cells, it has been shown that Zn^{2+} was transported either as a free ion via a saturable carrier-mediated process and an unsaturable pathway, or complexed with cysteine or histidine, via a sodium–amino acid cotransport mechanism [3]. More recent studies reported the expression of ZnT-1 transporter localized on the basolateral membrane and implicated it in the efflux of Zn^{2+} from the cytoplasm of intestinal and renal cells [4]. ZnT-2 is also an exporter present in intestine, kidney and testis, the role of which is to protect cells from zinc toxicity by facilitating zinc transport into an endosomal/lysosomal compartment [5,6]. ZnT-3 is probably involved in Zn^{2+} uptake in synaptic vesicles in brain [7] and ZnT-4 implicated in the extrusion of Zn^{2+} in mammary gland [8]. Concerning the uptake of Zn^{2+}, Gunshin et al. [9] have reported the cloning of the DCT1 proton-coupled metal-ion transporter which is highly expressed in the kidney. No studies report the characterization of metal transporters localized in the distal part of the tubule while it has been shown by microinjection studies the existence of such mechanisms [10]. Moreover, even if some of the transporters implicated in Zn^{2+} transport have been cloned, little is known about their functional properties. In this study, we used MDCK cells as a model of renal distal cells [11,12] to characterize a Zn^{2+} transport coupled to protons which could be implicated in the reabsorption of divalent cations in the distal part of the nephron.

2. Materials and methods

2.1. Culture conditions

Madin-Darby canine kidney (MDCK) cells were obtained from the American Type Culture Collection and used from passage 65 to 75. Cells were seeded on plastic Petri dishes at a concentration of 2×10^4 cells/cm^2 in DMEM-F12 mix

* Corresponding author. Fax: +33-4-92076850.
E-mail address: tauc@unice.fr (M. Tauc).

0005-2736/03/$ - see front matter © 2003 Elsevier Science B.V. All rights reserved.
doi:10.1016/S0005-2736(03)00052-X

containing 15 mM $NaHCO_3$, 20 mM Hepes (pH 7.2), 100 U/ml penicillin, 100 μg/ml streptomycin and 10% fetal calf serum. Cells were maintained at 37 °C in a 5% CO_2–air water saturated atmosphere.

2.2. Measurement of oxonol fluorescence

These experiments were performed on isolated cells. Isolated MDCK cells were harvested from confluent 100-mm Petri dishes by treatment with 2 ml trypsin–EDTA (10 ×) during 3 min. Then, cells were diluted in 50 ml of NaCl buffer, centrifuged to eliminate trypsin and finally suspended at a final concentration of 2×10^7 cells/ml in the appropriate buffer. Viability of the cells was assessed by eosin dye exclusion. Such a cell preparation presented an almost complete exclusion of eosin. All experiments were performed as previously described [13] with a Perkin Elmer LS-5 spectrofluorometer. Buffer (1.5 ml, in millimolars: NaCl 140, KCl 5, $CaCl_2$ 1, $MgCl_2$ 1, glucose 5, Hepes 20, pH 7.2) was added to a quartz cuvette maintained at 37 °C. Bis-oxonol (1,3-diethylthiobarbituric)trimethine oxonol (Molecular Probes) was prepared from a stock solution (15 mM in ethanol) at a concentration of 0.15 mM in H_2O and was added to the cuvette to give a final concentration of 0.15 μM. For each measurement, 10^6 cells were added and continuously stirred with a magnetic stirrer. Cells were excited at 540 nm and the emitted fluorescence at 580 nm was recorded. At the end of each experiment, 2 μM gramicidin D was added to the cuvette to fully depolarize the cells.

2.3. Correlation between emitted fluorescence and membrane potential

Isolated Madin-Darby canine kidney cells (10^6) were suspended in the cuvette of the spectrofluorometer in 1.5 ml of a solution containing 0.15 μM bis-oxonol in which the sodium was isoosmotically replaced by choline to various degrees. Emitted fluorescence at 580 nm was recorded and 1 μM gramicidin D was added. The relative fluorescence variations ($\Delta F/F_0$) recorded at various $[Na]_0$

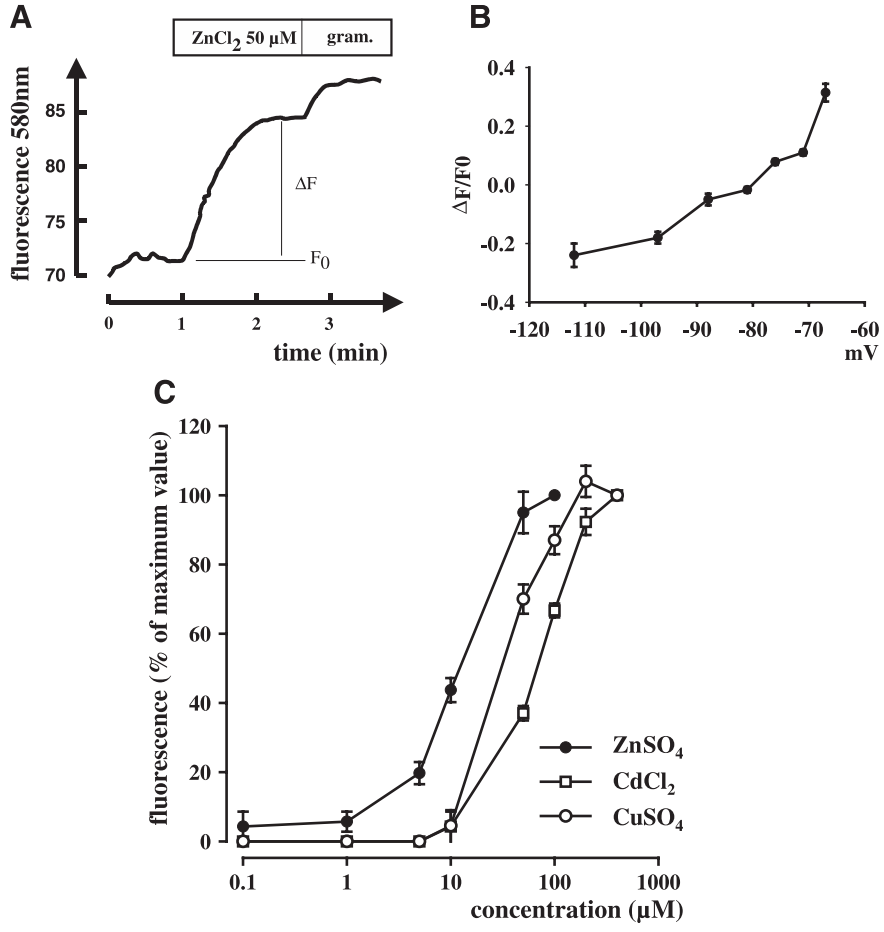

Fig. 1. Effect of trace elements on membrane potential. (A) Typical recording of oxonol-loaded MDCK cells in response to $ZnCl_2$. Cells (1×10^6) were suspended in 1.5 ml NaCl medium containing 0.15 μM bis-oxonol. Fifty micromolars $ZnCl_2$ was added at the indicated time. Fluorescence emitted at 580 nm was recorded along time and 1 μM gramicidin was added at the end of the experiment to fully depolarize cells. (B) Correlation between oxonol fluorescence and membrane potential determined as described in methods; each point is the mean ± S.E. of three experiments. (C) Dose-response curves obtained with $ZnCl_2$, $CdCl_2$ or $CuSO_4$. Results are expressed as the percentage of the maximum variation of the fluorescence signal obtained with each divalent cation; each point is the mean ± S.E. of three experiments.

were plotted against the membrane potential (Fig. 1A and B). The membrane potential was calculated assuming that the rates of Na^+ and K^+ permeation through the ionophore were similar using the equation: $Em=(RT/F)(\log[Na]_0/[Na_i+K_i])$(12). Na_i+K_i was determined by the null point method; it was equal to $[Na]_0$ when addition of gramicidin did not produce fluorescence change [13].

2.4. Whole-cell patch-clamp analysis

Whole-cell currents were recorded from MDCK cells grown on collagen-coated Petri dishes and bathed with a NaCl medium (in millimolars: NaCl 140, KCl 5, $CaCl_2$ 1, glucose 5, Hepes 10, pH 7.2). The ruptured-patch whole-cell configuration of the patch-clamp technique was used. Patch pipettes (resistance 2–3 MΩ) were made from borosilicate capillary tubes by using a two-stage vertical puller (Narishige) and filled with the following buffer (in millimolars): K-glutamate 110, NaCl 30, MgATP 5, Hepes 10, pH 7.4. Cells were observed with an inverted microscope, the stage of which was equipped with an electric micromanipulator. The patch pipette was connected via an Ag/AgCl wire to the headstage of a digital VP500 patch amplifier (Biologic, France). Voltage commands and data acquisition were controlled via a GPIB interface (Biologic) and data were analyzed by using Biopatch software. Cells were continuously maintained at a holding potential of − 40 mV.

2.5. ^{65}Zn uptake

Experiments were performed at 37 °C. The incubation medium contained (in millimolars): NaCl 140, KCl 5, $CaCl_2$ 1, Hepes 20, pH 7.2. The confluent MDCK cells grown on 12-well plates were rinsed three times with unlabelled medium and uptake was initiated by addition of 200 μl incubation medium containing 1 μCi/ml ^{65}Zn (Amersham). Uptake was stopped at 30 s by aspirating the medium and rinsing the wells three times with ice-cold phosphate-buffered saline containing 5 mM EGTA. All experiments were carried out in triplicate and the radioactivity was determined by scintillation counting after dissolving the cultured cells in 500 μl NaOH 0.1 N.

2.6. ^{22}Na uptake

The same protocol as for ^{65}Zn uptake was used except that 0.5 μCi/ml ^{22}Na was used and that the stop solution was composed of ice-cold 140 mM NaCl solution.

2.7. Measurement of intracellular pH

The pH variations were monitored by the measurement of BCECF fluorescence [14]. MDCK cells were loaded with 5 μM BCECF-AM during 15 min at 37 °C in culture medium. After rinsing in NaCl buffer (in millimolars: NaCl 140, KCl 5, $CaCl_2$ 1, $MgCl_2$ 1, glucose 5, Hepes 20, pH 7.2), monolayers were placed on the stage of an inverted microscope (Zeiss ICM 405 with a Zeiss 40× objective) coupled to a video camera. Fluorescence excitation was provided by a 75-W Xenon lamp (Osram), and was computer-controlled by a shutter. The excitation beam was filtered through 450 and 490 nm narrow band interference filters paired with appropriate quartz neutral-density filters mounted in a computer-controlled motorized wheel. Therefore, the cells were excited successively at 490 and 450 nm, and each image was digitalized and stored on the hard disk on the computer. Image treatment was performed using the Axon imaging workbench (AIW 4.0) software. This imaging program enables to quantify the pixel gray-level intensities for a maximum of 20 independent cells per experiments. At the end of the experimental series, the fluorescence signals relative to pHi were calibrated using

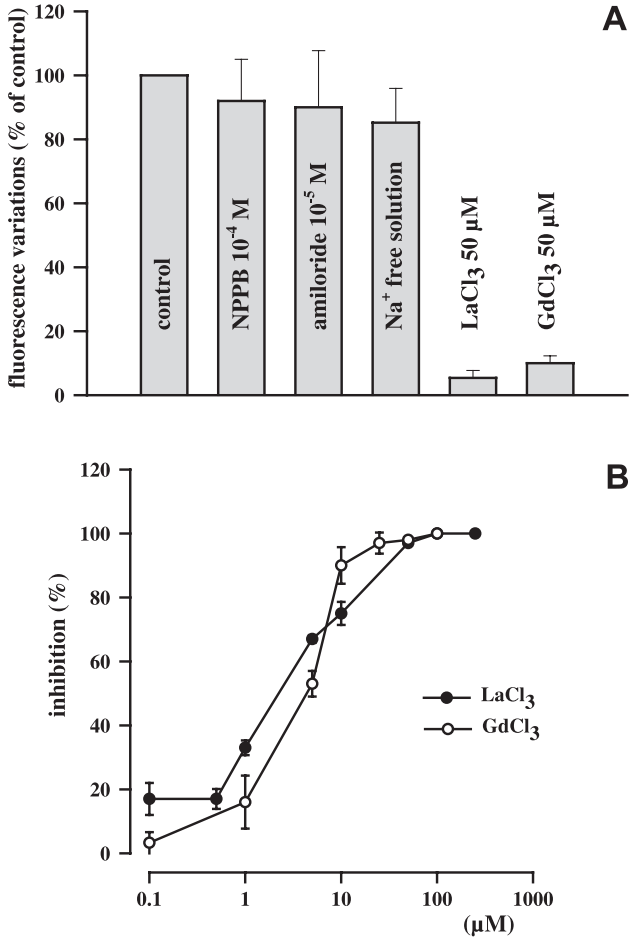

Fig. 2. Effect of inhibitors on the zinc-induced depolarization. Isolated MDCK cells were suspended in 1.5 ml buffer containing 0.15 μM bis-oxonol and 50 μM $ZnCl_2$ was added in the presence of 10^{-4} M NPPB ($n=3$), 10^{-5} M amiloride ($n=3$), 50 μM $GdCl_3$ ($n=3$), 50 μM $LaCl_3$ ($n=3$) or in the absence of Na^+ ($n=3$). (A) Results are expressed as the percentage of the maximum variation of the fluorescence signal obtained with 50 μM $ZnCl_2$ (control, $n=12$). Results are the mean ± S.E. of n experiments. (B) Dose-inhibition curves obtained with lanthanum and gadolinium. Each point is the mean ± S.E. of three experiments.

the K^+/H^+ exchanging ionophore nigericin [14]. For this purpose, the cells were perfused with KCl solutions (140 mM KCl, 20 mM Hepes and 10 μM nigericin) adjusted to pH 6.5, 7.0 and 7.5. From these measurements, a three-point calibration curve was constructed by plotting the grey-level ratios (490 nm/450 nm) as a function of the pH values. The pHi values were then obtained by linear interpolation of the values of the grey-level values and the calculated values were adjusted to the experimental calibration.

3. Results

3.1. Fluorescence variations induced by heavy metals in oxonol-loaded MDCK cells

We have previously shown [13] that oxonol could be used to monitor intracellular potential variations induced by external effectors. Addition of micromolar concentrations of Zn^{2+} induced an increase in the fluorescence of bis-oxonol-loaded MDCK cells. Bis-oxonol, a lipophilic anion, possesses physico-chemical properties that induce a change in fluorescence proportional to changes in membrane potential of oxonol-loaded MDCK cells as already demonstrated [13]. Fig. 1A shows a typical recording of the fluorescence measured at 580 nm after addition of zinc. Few seconds after the addition of 50 μM $ZnCl_2$, the fluorescence rapidly increases to reach a maximum within 1 min. Subsequent addition of the depolarizing ionophore gramicidin D (1 μM) further increases the fluorescence. Fig. 1B shows the ratio of the variation of fluorescence to the initial fluorescence as a function of the generated membrane potential. According to this calibration [13,15], the resting potential of MDCK cells was -80.2 ± 0.8 mV ($n=4$) and the maximum potential depolarization induced by Zn^{2+} was 11.1 ± 0.4 mV ($n=5$). We performed the

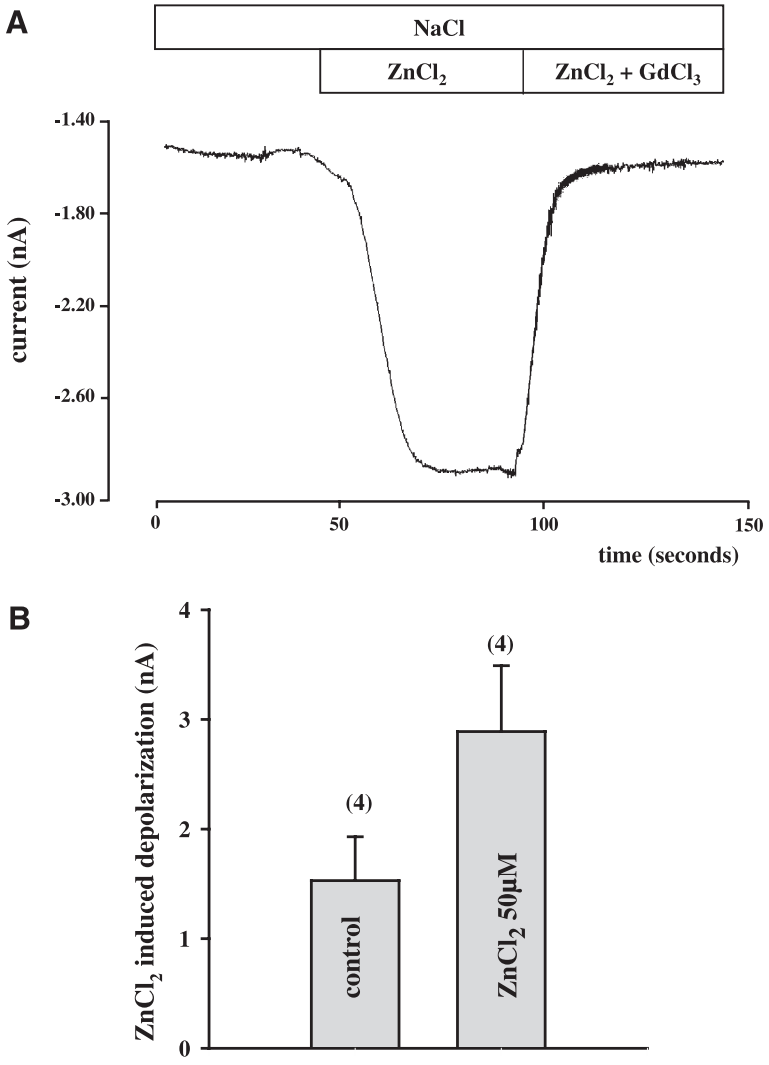

Fig. 3. Whole-cell recording of $ZnCl_2$-induced depolarization. (A) Typical recording; MDCK cells were maintained in the whole-cell configuration in NaCl medium at a holding potential of -40 mV. Fifty micromolars $ZnCl_2$ was added as indicated and current was recorded along time. Fifty micromolars $GdCl_3$ was then added in the presence of $ZnCl_2$ as indicated. (B) Amplitude of $ZnCl_2$-induced depolarization; results are the mean ± S.E. of n experiments.

same experiments with Cd^{2+} and Cu^{2+}. The maximum potential depolarizations obtained with this divalent cations were: Cd^{2+}: 9.2 ± 1 mV (n = 3), Cu^{2+}: 9.7 ± 0.8 mV (n = 3). Fig. 1C shows the dose-response curves obtained with Zn^{2+}, Cd^{2+} and Cu^{2+}. The results are expressed as the percentage of the maximum fluorescence variation obtained at saturating concentrations of the three different metals. Determined EC_{50} values were: 12 ± 2 μM for Zn^{2+}, 30 ± 4 μM for Cu^{2+} and 70 ± 5 μM for Cd^{2+}; n = 3. Co^{2+}, Mn^{2+} and Fe^{2+} were unable to induce any significant variations in oxonol fluorescence.

To further study the mechanism of Zn^{2+}-induced depolarization, we analyzed the oxonol response induced by zinc under different conditions. The histogram shown on Fig. 2A summarizes the results. Zn^{2+}-induced depolarization was not significantly modified by the addition of the chloride channel inhibitor 5-nitro-2-(3-phenylpropylamino)benzoic acid (NPPB, 10^{-4} M) or the sodium channel inhibitor amiloride (10^{-5} M). We also tested the effect of a Na^+-free medium. In these conditions, it appeared that the variation of the fluorescent signal was not modified as compared to the control condition in the presence of extracellular Na^+. Conversely, the addition of $LaCl_3$ or $GdCl_3$ inhibited the depolarization induced by $ZnCl_2$ in a dose-dependent manner as shown in Fig. 2A and B. IC_{50} values were: 2.0 ± 0.1 μM for $LaCl_3$ and 4.1 ± 0.5 μM for $GdCl_3$; n = 3. These data suggested that $ZnCl_2$ induced cell depolarization of MDCK cells by a mechanism which did not involve Cl^- or Na^+ channels and which is not dependent on extracellular Na^+.

3.2. Whole-cell patch-clamp analysis of zinc-induced depolarization

The results obtained with bis-oxonol-loaded cells suggest that Zn^{2+} activates an electrogenic mechanism. To verify this hypothesis, we performed whole-cell clamp experiments with MDCK cells seeded on Petri dishes. The ruptured-patch whole-cell configuration of the patch-clamp technique was used. Maintaining the cells at −40 mV resulted in an average current of −1.5 ± 0.4 nA; n = 4 (Fig. 3B). Addition of 50 μM $ZnCl_2$ induced an increase of the current to reach −2.9 ± 0.6 nA, n = 4 within 20 s as illustrated by the typical recording shown in Fig. 3A. Addition of 20 μM $GdCl_3$ during $ZnCl_2$ application made the current return near to the control value in few seconds (Fig. 3A). The effect of external pH on the Zn^{2+}-induced depolarization was tested. Results are illustrated in Fig. 4 which shows a typical experiment. The Zn^{2+}-induced depolarization current is strongly dependent on the extracellular pH, being increased at low pH.

3.3. Kinetic parameters of zinc uptake

To determine the kinetic parameters of Zn^{2+} transport, we performed ^{65}Zn uptake experiments. The relationship between ^{65}Zn uptake and increasing concentrations of zinc after 30 s incubation is shown in Fig. 5A. After the subtraction of the non-saturable component (3), the ^{65}Zn accumulation reached saturation above 60 μM. The kinetic parameters of zinc uptake obtained from these data are:

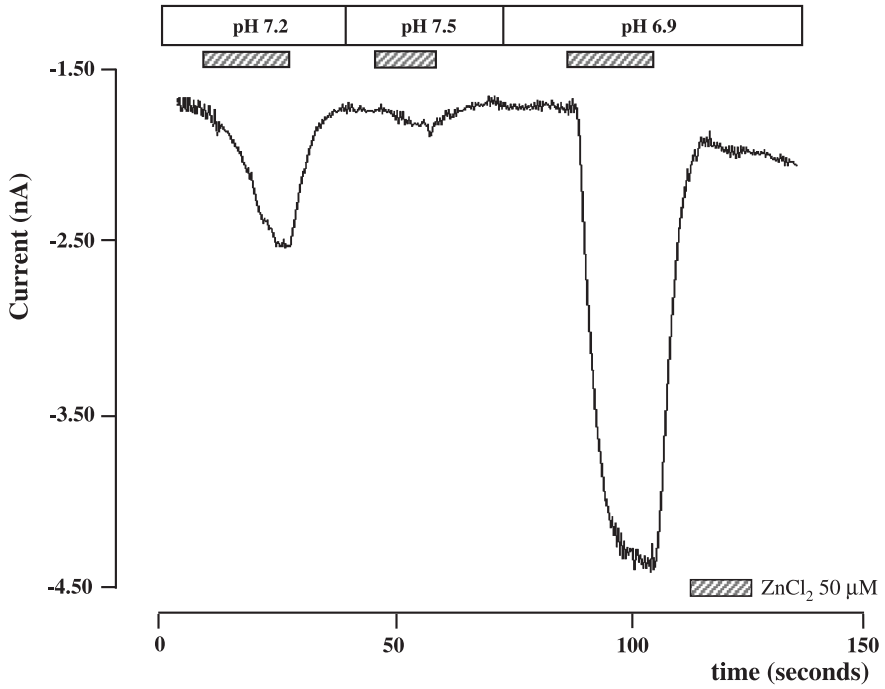

Fig. 4. Effect of extracellular pH on Zn^{2+}-induced depolarization. Typical recording; currents were recorded along time in the whole-cell configuration in NaCl medium buffered at different pHs (6.9, 7.2, 7.5) and maintained at a holding potential of −40 mV. Fifty micromolars $ZnCl_2$ was added as indicated.

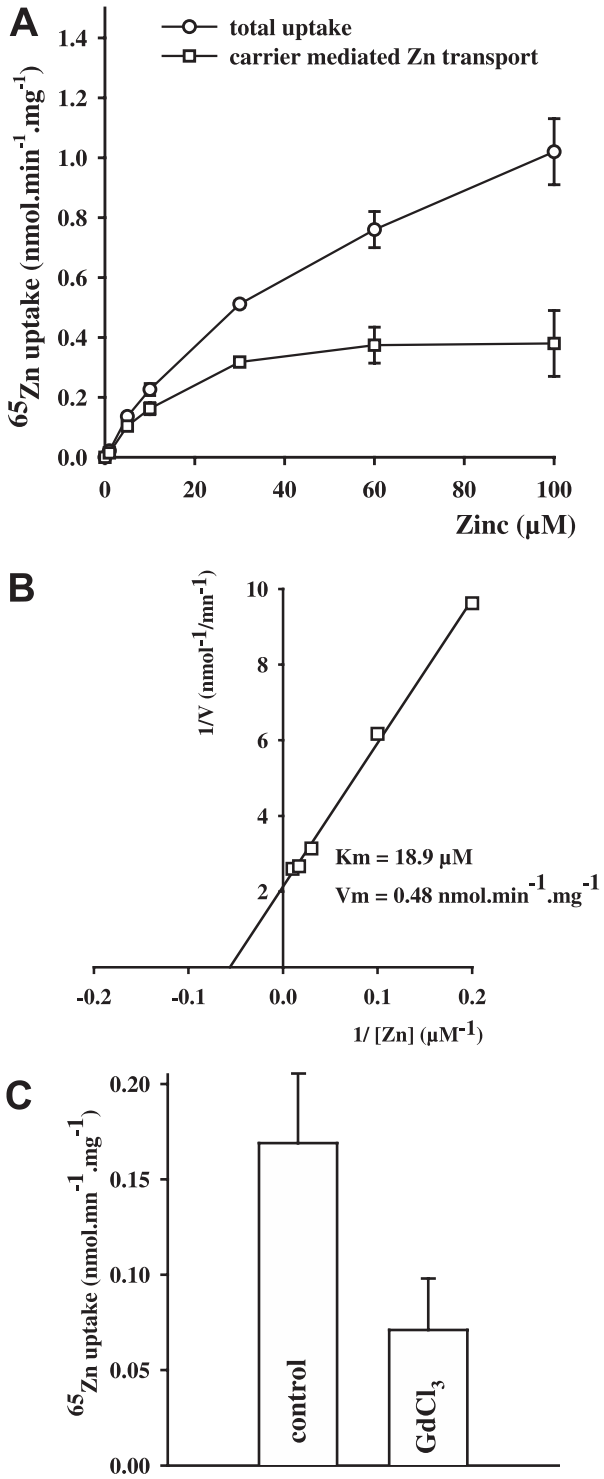

Fig. 5. Kinetic parameters of Zn^{2+} uptake. (A) Concentration dependence of ^{65}Zn uptake. Isolated MDCK cells were incubated for 0.5 min at 37 °C and increasing external Zn concentration. The unsaturable component was subtracted from the total uptake (○) to obtain the carrier-mediated transport (□). Each point represents the mean ± S.E. of triplicate samples from three different cultures. (B) Lineweaver–Burk linearization of data obtained from A. (C) Effect of 10 µM $GdCl_3$ on ^{65}Zn uptake after 30 s incubation at 100 µM external zinc. Results are the mean ± S.E. of three experiments.

$V_{max} = 0.48$ nmol min^{-1} (mg $protein^{-1}$), $K_m = 18.9$ µM at 37 °C (Fig. 5B). The effect of $GdCl_3$ was tested on the uptake of 100 µM Zn^{2+}. Fig. 5C shows that 10 µM $GdCl_3$ inhibited ^{65}Zn uptake by 58% [control: 0.169 ± 0.036; $GdCl_3$: 0.071 ± 0.026 nmol min^{-1} (mg $protein^{-1}$) $n = 3$].

3.4. Intracellular acidification induced by zinc uptake

In the past years, Gunshin et al. [9] have cloned a proton-coupled metal-ion transporter (DCT1) from rat duodenum which allowed for the intracellular uptake of heavy metals together with protons. This transporter is highly expressed in the kidney [16] and, to look for the existence of a similar mechanism in MDCK cells, we measured the intracellular pH variations induced by Zn^{2+}. For this purpose, we used the BCECF fluorescence technique coupled to image analysis on monolayers of MDCK cells. Results are shown in Fig. 6. After an initial period of stabilization in NaCl buffer, the addition of 50 µM $ZnCl_2$ induced a rapid decrease of intracellular pH within minutes (initial pH: 7.3 ± 0.01; lower pH: 6.85 ± 0.02, $n = 9$). Upon removal of $ZnCl_2$, intracellular pH returned toward the control value (final pH = 7.1 ± 0.03, $n = 9$). Addition of 10 µM 5-(*N*-ethyl-*N*-isopropyl)-amiloride (EIPA, a potent inhibitor of the Na^+/H^+ antiporter) during the wash-out of $ZnCl_2$ completely inhibited pH recovery (final pH = 6.89 ± 0.03, $n = 6$). To verify that Zn^{2+}-induced acidification was not due to an intracellular effect of the metal, we performed experiments in which cells were treated with 20 µM Zn^{2+} ionophore Na pyrithione (1-hydroxypyridine 2-thione, Sigma) before $ZnCl_2$ addition [17]. In these conditions, where Zn^{2+}

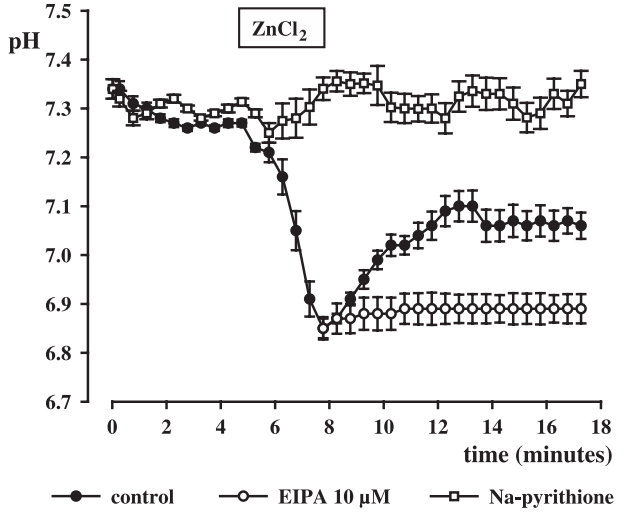

Fig. 6. Intracytoplasmic acidification induced by zinc. MDCK cells were loaded with 15 µM BCECF for 15 min at 37 °C and rinsed in NaCl medium. One hundred micromolars $ZnCl_2$ was added during the time indicated in the bar. The pH was determined as described in methods in control conditions (●, $n = 9$) or in the presence of 10 µM EIPA (○, $n = 6$). □: 20 µM Zn^{2+} ionophore Na pyrithione was added before the addition of $ZnCl_2$ ($n = 5$). Each point is the mean ± S.E. of n cells from two different cultures.

entered freely the cells, no acidification could be observed (Fig. 6). This result confirmed the fact that intracellular acidification was due to an extracellular uptake of protons coupled to Zn^{2+} entry.

3.5. Role of extracellular sodium

The mechanism implicated in the pH recovery after $ZnCl_2$ acidification depends on an EIPA-sensitive mechanism. To demonstrate that Na^+/H^+ exchanger mediates this alkalinization, we performed ^{22}Na uptake experiments. In control conditions, the basal ^{22}Na uptake saturated within the range 70–140 mM (Fig. 7A). This uptake was enhanced in the presence of 50 μM $ZnCl_2$: [control: 17.3 ± 3.1; $ZnCl_2$: 74.0 ± 2.9 nmol min^{-1} (mg $protein^{-1}$)] for an extracellular Na^+ concentration of 140 mM. We also measured the ^{22}Na uptake as a function of extracellular $ZnCl_2$ in the presence or the absence of 1 mM amiloride in the incubation medium. The results are shown in Fig. 7B. In control conditions, ^{22}Na uptake was dependent on the external zinc concentration up to 100 μM and was strongly inhibited by 1 mM amiloride. Fig. 8 summarizes some of the pharmacological properties of the Zn^{2+}-induced ^{22}Na uptake. As compared to control, 50 μM $ZnCl_2$ induced a 6-fold increase in Na^+ uptake. This uptake was only inhibited at a high amiloride concentration. The sodium uptake was significantly inhibited by 50 μM $GdCl_3$ and 50 μM $LaCl_3$. This inhibition of the sodium uptake was not due to a direct inhibition of the Na^+/H^+ exchanger but may be due to the indirect effect of these inhibitors on the proton-coupled Zn^{2+} transporter which was therefore unable to acidify cells.

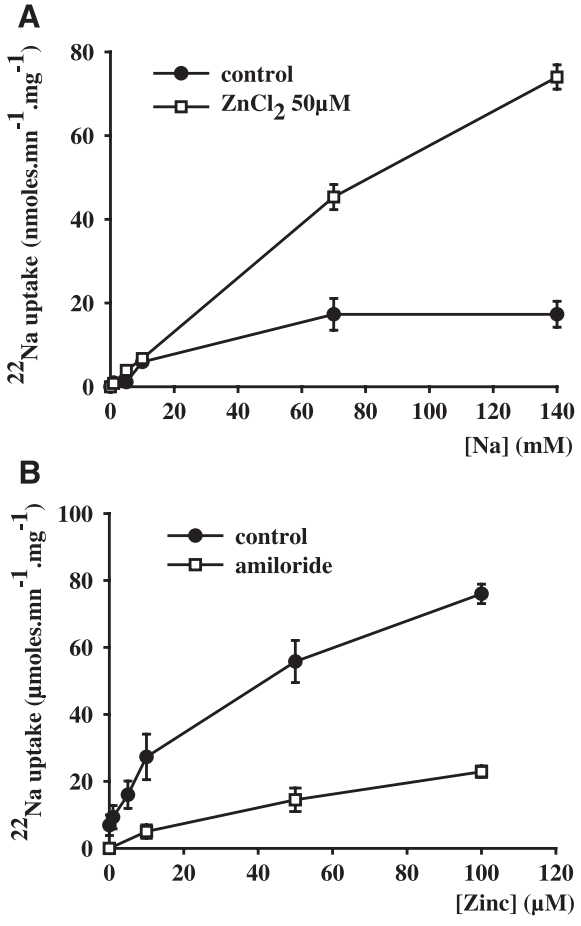

Fig. 7. Characteristics of Na^+ transport. (A) Concentration dependence of ^{22}Na uptake. Isolated MDCK cells were incubated for 0.5 min at 37 °C and increasing external Na^+ concentration. ^{22}Na uptake was performed in the presence or the absence of 50 μM $ZnCl_2$. (B) Uptake of ^{22}Na as a function of increasing concentrations of zinc in the presence or the absence of 1 mM amiloride. Each point represents the mean ± S.E. of triplicate samples from three different cultures.

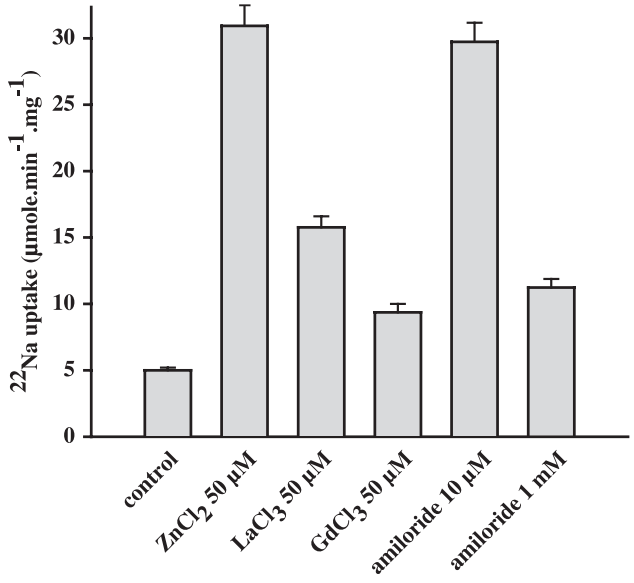

Fig. 8. Pharmacology of Na^+ transport. $^{22}Na^+$ uptake was performed at 140 mM extracellular Na^+ for 0.5 min at 37 °C in various conditions in the presence of 50 μM $ZnCl_2$. Control condition represents $^{22}Na^+$ uptake in the absence of zinc. Values are mean ± S.E. of three experiments.

4. Discussion

In the present paper, we demonstrate the expression of a proton-coupled Zn^{2+} transporter in MDCK cells. Few studies concerned metal transport in these cells which could be considered as a model of distal tubular cells [11,12]. However, we must consider the work of Nagao et al. [18] who have evidenced for the existence of a unidirectional transport of cobalt which involved an apical transporter with a broad specificity. The results obtained by these authors showed that zinc was able to inhibit this cobalt transport and demonstrated also that other zinc pathways through which Co^{2+} is not transported exist in the apical membrane of MDCK cells. Another work reports the characterization of a cadmium transport inhibited by Fe and regulated by protein kinase C [19]. In our study, we found an electrogenic metal system transport able to depolarize MDCK cells, activated by Zn^{2+}, Cd^{2+} and Cu^{2+} and inhibited by gadolinium and

lanthanum. Conversely, Fe^{2+}, Co^{2+} or Mn^{2+} failed to depolarize cells. The finding that zinc-induced depolarization was not inhibited by NPBB or amiloride excluded any direct activation of Cl^- or Na^+ channels by Zn^{2+}. ^{65}Zn uptake experiments demonstrated the presence of a zinc saturable transport and suggested that cell depolarization was probably due to Zn^{2+} uptake. This is reinforced by the fact that Zn^{2+} transport as well as Zn^{2+} depolarization was inhibited by the same inhibitor gadolinium. To further characterize the transporter, we performed experiments in the absence of extracellular Na^+. This maneuver did not modify the Zn^{2+}-induced cell depolarization, allowing us to exclude any Na^+-coupled cotransport system. Such an influence of Na^+ in Zn^{2+} transport was already demonstrated in isolated proximal cells where Zn^{2+} has been shown to enter the cells partly complexed with cysteine or histidine, by means of a sodium/amino acid cotransport mechanism [3]. In another series of experiments, we looked for an effect of external pH on the depolarization induced by Zn^{2+}. It appears that the depolarization is stimulated at low pH, suggesting either that the transporter is sensitive to external pH or that the driving force is generated by the proton gradient. The last hypothesis is very likely because our data demonstrated clearly that addition of Zn^{2+} on MDCK cells induced intracellular acidification and that this acidification was not due to an intracellular effect consecutive to Zn^{2+} entry but was the result of an uptake of external protons. In turn, this intracellular acidification activated Na^+/H^+ exchanger that participated in proton recycling. A proton-coupled metal transporter (DCT1) has been cloned by Gunshin et al. [9] and could transport a large variety of divalent cations including Fe^{2+}, Zn^{2+}, Cd^{2+}, Mn^{2+}, Co^{2+}, Cu^{2+}, Ni^{2+} and Pb^{2+}. According to these authors, DCT1 is expressed in the kidney mainly in S3 proximal tubule segments and is the first mechanism potentially responsible of metal uptake and characterized in mammals. More recently, Ferguson et al. [16] have also demonstrated the high level of expression of DCT1 in the distal part of the rat nephron including distal convoluted tubule and cortical collecting duct. DCT1 has high homology to the Nramp family of genes implicated in host defense mechanism and the up-regulation of its expression by iron deficiency supports a role for DCT1 in metal transport. A divalent cation transporter coupled to protons and similar to DCT1 has also been identified in Caco-2 cells [20] and in intestinal brush border membrane [21]. Separately, a metal transporter sensitive to proton gradient has been characterized from rat renal brush border membrane [2]. Once reconstituted in proteo-liposomes, this zinc transporter of 40 kDa exhibited a relatively low affinity for Zn^{2+} ($K_m = 1.03$ mM) with an initial uptake velocity of Zn^{2+} uptake increased by the increase in outwardly directed proton gradient. Recently, another family of protein has been shown to be implicated in Zn^{2+} cell uptake into human cells. These transporters (hZIP1 and hZIP2) belong to the ZIP superfamily of transporters, which are expressed in diverse organisms. hZIP2 is only expressed in the plasma membrane of prostate and uterine cells [22] and was shown to work as a HCO_3-Zn^{2+} cotransporter. hZIP1 is widely expressed in numerous organs [23] but its relation with HCO_3^- is not clearly established. Nevertheless, in MDCK cells, Zn^{2+} uptake leads to an intracellular acidification and it is likely that it is not mediated through mechanism involving an hZIP-like protein, which is presumed to alkalinize the cells due to the coupling with HCO_3^-. The Zn^{2+} uptake mechanism we describe in MDCK cells is similar to DCT1 as far as electrogenicity and coupling with protons are concerned. However, in MDCK cells, the inability of Fe^{2+}, Co^{2+} or Mn^{2+} to depolarize MDCK cells suggests large differences in the specificity of the transporter we describe as compared to DCT1. Two studies reinforce the fact that the mechanism we describe could be different from DCT1: Sacher et al. [24] have demonstrated that once expressed in *Xenopus oocytes*, DCT1 was unable to transport Zn^{2+} and in the same way, Tandy et al. [20] have demonstrated that DCT1 was not responsible of Zn^{2+} transport in Caco-2 cells. Finally, MDCK cells could represent a good model of metal transport localized in the distal part of the nephron which have been shown implicated in divalent cation transport [10]. Coupling of Zn^{2+} transport with protons leads to intracellular acidification, which activates the Na^+/H^+ exchanger, allowing for the recycling of protons and the sustained uptake of Zn^{2+}. This mechanism could be physiologically relevant in the distal parts of the renal tubule in which the inward gradient of protons is increased due to the lower pH of the tubular fluid.

References

[1] J.G. Reyes, Zinc transport in mammalian cells, Am. J. Physiol. 270 (1996) C401–C410.
[2] R. Kumar, R. Prasad, Functional characterization of purified zinc transporter from renal brush border membrane of rat, Biochim. Biophys. Acta 1509 (2000) 429–439.
[3] B. Gachot, M. Tauc, L. Morat, P. Poujeol, Zinc uptake by proximal cells isolated from rabbit kidney: effects of cysteine and histidine, Pflugers Arch. 419 (1991) 583–587.
[4] R.D. Palmiter, S.D. Findley, Cloning and functional characterization of a mammalian zinc transporter that confers resistance to zinc, EMBO J. 14 (1995) 639–649.
[5] R.J. McMahon, R.J. Cousins, Mammalian zinc transporters, J. Nutr. 128 (1998) 667–670.
[6] R.D. Palmiter, T.B. Cole, S.D. Findley, ZnT-2, a mammalian protein that confers resistance to zinc by facilitating vesicular sequestration, EMBO J. 15 (1996) 1784–1791.
[7] R.D. Palmiter, T.B. Cole, C.J. Quaife, S.D. Findley, ZnT-3, a putative transporter of zinc into synaptic vesicles, Proc. Natl. Acad. Sci. U. S. A. 93 (1996) 14934–14939.
[8] R.J. Cousins, R.J. McMahon, Integrative aspects of zinc transporters, J. Nutr. 130 (2000) 1384S–1387S.
[9] H. Gunshin, B. Mackenzie, U.V. Berger, Y. Gunshin, M.F. Romero, W.F. Boron, S. Nussberger, J.L. Gollan, M.A. Hediger, Cloning and characterization of a mammalian proton-coupled metal-ion transporter, Nature 388 (1997) 482–488.
[10] M. Wareing, C.J. Ferguson, R. Green, D. Riccardi, C.P. Smith, In vivo characterization of renal iron transport in the anaesthetized rat, J. Physiol. 524 (Pt 2) (2000) 581–586.

[11] D.A. Herzlinger, T.G. Easton, G.K. Ojakian, The MDCK epithelial cell line expresses a cell surface antigen of the kidney distal tubule, J. Cell Biol. 93 (1982) 269–277.
[12] M.J. Rindler, L.M. Chuman, L. Shaffer, M.H. Saier Jr., Retention of differentiated properties in an established dog kidney epithelial cell line (MDCK), J. Cell Biol. 81 (1979) 635–648.
[13] M. Tauc, M. Gastineau, P. Poujeol, Toxin pharmacology of the ATP-induced hyperpolarization in Madin-Darby canine kidney cells, Biochim. Biophys. Acta 1105 (1992) 155–160.
[14] M. Bidet, M. Tauc, N. Koechlin, P. Poujeol, Video microscopy of intracellular pH in primary cultures of rabbit proximal and early distal tubules, Pflugers Arch. 416 (1990) 270–280.
[15] S. Grinstein, J.D. Goetz, A. Rothstein, 22Na+ fluxes in thymic lymphocytes: I. Na+/Na+ and Na+/H+ exchange through an amiloride-insensitive pathway, J. Gen. Physiol. 84 (1984) 565–584.
[16] C.J. Ferguson, M. Wareing, D.T. Ward, R. Green, C.P. Smith, D. Riccardi, Cellular localization of divalent metal transporter DMT-1 in rat kidney, Am. J. Physiol., Renal Physiol. 280 (2001) F803–F814.
[17] S.L. Sensi, L.M. Canzoniero, S.P. Yu, H.S. Ying, J.Y. Koh, G.A. Kerchner, D.W. Choi, Measurement of intracellular free zinc in living cortical neurons: routes of entry, J. Neurosci. 17 (1997) 9554–9564.
[18] M. Nagao, E. Sugaru, T. Kambe, R. Sasaki, Unidirectional transport from apical to basolateral compartment of cobalt ion in polarized Madin-Darby canine kidney cells, Biochem. Biophys. Res. Commun. 257 (1999) 289–294.
[19] L. Olivi, J. Sisk, J. Bressler, Involvement of DMT1 in uptake of Cd in MDCK cells: role of protein kinase C, Am. J. Physiol., Cell Physiol. 281 (2001) C793–C800.
[20] S. Tandy, M. Williams, A. Leggett, M. Lopez-Jimenez, M. Dedes, B. Ramesh, S.K. Srai, P. Sharp, Nramp2 expression is associated with pH-dependent iron uptake across the apical membrane of human intestinal Caco-2 cells, J. Biol. Chem. 275 (2000) 1023–1029.
[21] M. Knopfel, G. Schulthess, F. Funk, H. Hauser, Characterization of an integral protein of the brush border membrane mediating the transport of divalent metal ions, Biophys. J. 79 (2000) 874–884.
[22] L.A. Gaither, D.J. Eide, Functional expression of the human hZIP2 zinc transporter, J. Biol. Chem. 275 (2000) 5560–5564.
[23] L.A. Gaither, D.J. Eide, The human ZIP1 transporter mediates zinc uptake in human K562 erythroleukemia cells, J. Biol. Chem. 276 (2001) 22258–22264.
[24] A. Sacher, A. Cohen, N. Nelson, Properties of the mammalian and yeast metal-ion transporters DCT1 and Smf1p expressed in *Xenopus laevis* oocytes, J. Exp. Biol. 204 (2001) 1053–1061.